A Multiparametric MRI-Based Scoring System for Differentiation Between Pseudoprogression and True Progression in High-Grade Glioma

Mohammad Ghorbani (PhD Candidate)[1], Mohammad Ali Oghabian (PhD)[1,2]*, Samira Raminfard (PhD)[2,3], Nahid Sadighi (MD)[3,4], Mostafa Farzin (MD)[5,6]

[1]Department of Medical Physics and Biomedical Engineering, School of Medicine, Tehran University of Medical Sciences, Tehran, Iran
[2]Neuroimaging and Analysis Group, Research Center for Molecular and Cellular Imaging, Advanced Medical Technologies and Equipment Institute, Tehran University of Medical Sciences, Tehran, Iran
[3]Advanced Diagnostic and Interventional Radiology Research Center (ADIR), Imam Khomeini Complex Hospital, Tehran University of Medical Sciences, Tehran, Iran
[4]Medical Imaging Center of Imam Khomeini Hospital Complex (IKHC), Tehran University of Medical Sciences, Tehran, Iran
[5]Department of Radiation Oncology, Cancer Institute, IKHC, School of Medicine, Tehran University of Medical Sciences, Tehran, Iran
[6]Brain and Spinal Cord Injury Research Center, Neuroscience Institute, Tehran University of Medical Science, Tehran, Iran

*Corresponding author: Mohammad Ali Oghabian
Department of Medical Physics and Biomedical Engineering, School of Medicine, Tehran University of Medical Sciences, Tehran, Iran
E-mail: oghabian@sina.tums.ac.ir

Received: 4 March 2025
Accepted: 28 April 2025

ABSTRACT

Background: Differentiating Pseudoprogression (PSP) from True Progression (TP) in High-Grade Gliomas (HGGs) is challenging. Integrating parameters from advanced Magnetic Resonance Imaging (MRI) techniques may improve diagnostic performance.

Objective: Integrating multiparametric MRI (mp-MRI) with a Multiparametric Scoring System (MSS) may improve PSP-TP differentiation.

Material and Methods: In this prospective study, thirty HGG patients with post-standard treatment underwent mp-MRI on a 3T system, including Dynamic Susceptibly Contrast (DSC) MRI, Intravoxel Incoherent Motion (IVIM) MRI, Magnetic Resonance Spectroscopy (MRS), and anatomical imaging. Parametric maps were extracted, registered to anatomical images, and analyzed within a Volume of Interest (VOI) on the enhancing lesion in post-contrast T1-weighted images. Mean VOI values were compared between PSP and TP groups. Statistical analysis identified significant parameters, their Area Under the Curve's (AUC), and optimal cutoffs, used to assign binary scores (0 or 1) and calculate a sum score for each patient. The diagnostic performance of the sum score was assessed using Receiver Operating Characteristic (ROC) curve analysis against a reference standard determined by follow-up MRI or histopathology when available.

Results: nCBV, nCBF, and nMTT from DSC MRI, normalized-D* from IVIM-MRI, and normalized-Cho/Cr from MRS exhibited significantly higher values in the TP group. Normalized-D and -ADC from IVIM-MRI were significantly elevated in the PSP group. The MSS approach, integrating these parameters into a sum score, demonstrated high diagnostic performance with 0.958 AUC, 87.5% sensitivity, and 92.9% specificity for distinguishing PSP from TP.

Conclusion: Addressing the limitations of single-parameter MRI approaches, the MSS method effectively integrates mp-MRI parameters to distinguish PSP from TP in HGG patients, enhancing diagnostic performance.

Keywords

Multiparametric Magnetic Resonance Imaging; Glioma; Brain Neoplasms; Multiparametric Scoring System; Pseudoprogression; Treatment Assessment

Introduction

High-Grade Gliomas (HGGs) represent one of the most formidable challenges in oncology due to their aggressive nature and poor prognosis, with survival rates remaining low despite

advancements in treatment. The standard of care involves maximal or supramaximal resection, followed by radiotherapy and temozolomide chemotherapy. However, accurately assessing treatment response remains a major challenge, particularly in distinguishing True Progression (TP) from Pseudoprogression (PSP) [1], which is a transient imaging phenomenon that closely mimics TP on Magnetic Resonance Imaging (MRI), complicating clinical decision-making. This diagnostic challenge is further exacerbated by the temporal overlap of PSP and TP imaging features, particularly in the early months following radiotherapy and chemotherapy, when treatment-induced inflammatory changes can mimic tumor progression, complicating accurate differentiation. During this period, both conditions may present with increased contrast enhancement and peritumoral edema, increasing the risk of misclassification [2, 3].

Given these diagnostic challenges, misdiagnosis of PSP or TP can have serious consequences. Mistaking PSP for TP might lead to unnecessary treatments, while confusing TP for PSP could delay essential care. Therefore, accurate diagnosis is crucial for effective treatment and better patient outcomes [4]. While conventional MRI sequences remain a cornerstone of brain tumor imaging, their well-documented limitations in differentiating PSP from TP underscore the need for complementary techniques [5].

In clinical practice and research, advanced MRI sequences, such as perfusion-weighted MRI, diffusion-weighted MRI, and Magnetic Resonance Spectroscopy (MRS) have been widely used to distinguish PSP from TP in high-grade gliomas [2]. Quantitative parameters derived from these sequences provide valuable insights into tumor characteristics, with each technique offering specific advantages [6]. Although some studies have successfully used individual MRI parameters to differentiate between PSP and TP [7, 8], depending solely on one parameter may fail to address the multifaceted and heterogeneous behavior of gliomas and their responses to treatment [9]. As a result, there is an increasing recognition that a more comprehensive approach, capable of integrating multiple MRI parameters, may provide a better diagnostic framework.

To address these limitations, the use of multiparametric MRI has gained attention as an effective method for distinguishing PSP from TP in high-grade gliomas [10]. By combining several MRI parameters, each derived from different advanced sequences, the multiparametric approach offers a more robust and comprehensive assessment of the tumor microenvironment. This method provides a more complete picture of tumor biology and treatment effects, allowing clinicians to account for the complex interactions between various physiological and molecular processes that cannot be captured by a single parameter alone [9]. Recent studies have demonstrated that integrating multiple parameters improves diagnostic accuracy, as it reduces the risk of misclassification that may arise from relying on a single MRI sequence [11].

Building on the advantages of multiparametric MRI, the Multiparametric Scoring System (MSS), introduced by Matsusue [12], provides a simple yet effective approach for integrating MRI parameters into a clinically applicable score. Unlike methods that rely on a single MRI parameter, MSS incorporates multiple significant parameters from different advanced MRI sequences, allowing for a more comprehensive tumor assessment.

Given the critical importance of accurate differentiation in optimizing treatment strategies and improving patient outcomes, this study aims to evaluate whether combining MRI parameters from a multiparametric MRI protocol can effectively distinguish PSP from TP in high-grade glioma patients and whether the MSS method offers improved classification accuracy compared to single-parameter approaches.

In this study, the proposed MSS builds upon the approach introduced by Matsusue [10], incorporating additional MRI parameters, particularly Intravoxel Incoherent Motion (IVIM) metrics, to evaluate the possibility of enhanced diagnostic performance. Moreover, while Matsusue's study included glioma patients across all grades, this study focused exclusively on patients with HGG to improve cohort homogeneity and strengthen the reliability of our findings in this specific population.

Material and Methods

Study Population

This single-center and prospective study was conducted in accordance with the Declaration of Helsinki and approved by the Tehran University of Medical Sciences. The study was performed at the Medical Imaging Center, Imam Khomeini Hospital, Tehran, between December 2020 and March 2023. Patients with histopathologically confirmed World Health Organization (WHO) grade III or IV high-grade gliomas, who had completed standard treatment (surgery, radiotherapy, and chemotherapy), were considered for inclusion.

Eligibility criteria required a pre-treatment histopathological diagnosis of high-grade glioma, completion of the standard treatment regimen, and the availability of multiparametric MRI within six months after completing therapy. Follow-up MRI examinations were performed at 2- to 4-month intervals, with a minimum follow-up of 12 months (range: 12-18 months) for patients classified based on imaging. The PSP was defined as a decrease in enhancing lesion size or stability on follow-up imaging, while TP was defined as a progressive increase in enhancing lesion size.

A total of 41 patients were enrolled; however, 11 were excluded due to poor image quality (e.g., motion artifacts, n=4), absence of enhancing lesions (n=3), or failure to complete follow-up MRI (n=4). Ultimately, 30 patients (16 females, 14 males; mean age ±SD: 47±15.58 years) met the inclusion criteria. Among these, 22 patients had WHO grade IV gliomas, and 8 had WHO grade III gliomas. Based on histopathological confirmation in five cases and follow-up MRI findings in the remaining 25 cases, patients were classified into two groups: PSP (n=14) and TP (n=16).

MRI Acquisition

Brain imaging was performed on a 3T scanner (Discovery MR750W; GE Healthcare) and included both conventional and advanced MRI sequences. Conventional MRI consisted of pre- and post-contrast T1-weighted, T2-weighted, and Fluid-Attenuated Inversion Recovery (FLAIR) sequences, with detailed settings provided in Table 1. Post-contrast T1-weighted imaging followed the intravenous injection of 0.1 mmol/kg gadolinium (DOTAREM; Guerbet, France). Advanced techniques included IVIM MRI, Dynamic Susceptibly Contrast (DSC) MRI, and MRS.

IVIM MRI was acquired before contrast injection using 11 b-values (0, 20, 40, 60, 80, 100, 200, 400, 600, 800, and 1000 s/mm^2) in three orthogonal directions. Eleven b-values were selected based on literature recommendations to optimize the estimation of both diffusion and perfusion parameters in IVIM MRI [13]. For DSC MRI, a standardized contrast protocol was employed, with a dose of 0.1 mmol/kg gadolinium injected intravenously at a rate of 4 ml/sec, beginning at time point 15 of the perfusion acquisition. The sequence included a total of 90 time points, ensuring adequate temporal resolution for perfusion analysis. The specific sequence settings for IVIM MRI and DSC MRI are also shown in Table 1.

MRS was performed after contrast administration, following DSC MRI and post-contrast T1-weighted sequences. To comprehensively assess lesion metabolism, a combination of Single-Voxel (SV), 2D-Chemical Shift Imaging (2D-CSI), and 3D-CSI was initially considered. Although 2D-CSI and 3D-CSI provide broader tissue coverage, their larger field

of view increases susceptibility to magnetic field inhomogeneities. In the studied patients, post-surgical brain alterations, the proximity of enhancing lesions to the skull base, and the presence of bone-air interfaces exacerbated these effects, resulting in degraded spectral quality [14, 15]. Given these limitations, SV-MRS, which offers greater flexibility in voxel placement and is less affected by these confounding factors, was selected as the primary MRS acquisition method in this study. Voxels were carefully positioned within the enhancing portion of the lesion and in contralateral normal-appearing brain tissue, avoiding areas prone to magnetic field distortions. Spatially localized saturation bands and automatic shimming with water suppression were applied to minimize signal contamination from subcutaneous lipid and bone. This approach reduced interference from surrounding tissues and enhanced magnetic field uniformity around the target voxel, improving spectral quality.

In this study, MRI sequences were selected for their complementary roles in assessing tumor characteristics. DSC MRI evaluates tumor vascularity and hemodynamics, IVIM MRI provides insights into tissue diffusion and microvascular perfusion, and MRS assesses metabolic alterations. By combining these techniques, this study aimed to capture distinct physiological and metabolic features to improve differentiation between PSP and TP.

MR data Postprocessing

MRI data postprocessing was meticulously performed under the supervision of a neuroradiologist with over 15 years of experience, who was blinded to the final diagnostic results. The analysis involved the following steps:

DSC MRI Parametric Map Generation

To ensure accurate perfusion parameter estimation, rigorous preprocessing steps were applied to the perfusion data before generating parametric maps (Cerebral Blood Volume (CBV), Cerebral Blood Flow (CBF), and

Table 1: MRI acquisition parameters setting for different sequences used in the study, including T2-weighted, T1-weighted (pre- and post-contrast), FLAIR, IVIM MRI, DSC MRI, and SV-MRS.

Sequence	Plane	TR/TE/TI (ms)	FOV (mm^2)	Slice Thickness / Gap (mm)	Flip Angle (°)	#b-values	#Time Points	Other Parameters
T2-weighted	Axial	5500/100/-	220×220	4.5 / 1	90	-	-	-
T1-weighted	Axial	600/10/-	220×220	4.5 / 1	90	-	-	-
FLAIR	Axial	9000/136/2468	220×220	4.5 / 1	90	-	-	-
IVIM MRI	Axial	3000/90/-	240×240	4.5 / 1	90	11	-	b-values: 0, 20, 40, 60, 80, 100, 200, 400, 600, 800, 1000 s/mm^2
DSC MRI	Axial	1500/45/-	240×240	5 / 1	60	-	90	Gadolinium- (0.1 mmol/kg), Injection Rate: 4 mL/s
SV-MRS	Single Voxel	1500/144/-	240×240	-	90	-	-	Voxel Size: 1.7×1.7×1.7 cm^3

FLAIR: Fluid-Attenuated Inversion Recovery, IVIM: Intravoxel Incoherent Motion, MRI: Magnetic Resonance Imaging, DSC: Dynamic Susceptibility Contrast, SV-MRS: Single Voxel Magnetic Resonance Spectroscopy, TR: Time of Repetition, TE: Time of Echo, TI: Time of Inversion, FOV: Field of View

Mean Transit Time (MTT)) using NordicICE 4.2.0 software, as follows: 1) motion correction: A rigid co-registration method was employed to mitigate head motion during acquisition, 2) noise filtering: a predefined threshold was set to exclude non-brain pixels, 3) temporal smoothing: applied to reduce noise and signal spikes in the dynamic response, 3) pre-bolus range detection: ensured accurate delineation of the pre-contrast phase, and 4) initial time point exclusion: early time points were removed due to signal instability before reaching a steady state.

After preprocessing, the Arterial Input Function (AIF) was determined using an unsupervised global detection method based on R2* relaxation rate curve characteristics. Perfusion parametric maps were then generated using standard Singular Value Decomposition (sSVD) with a fixed regularization parameter of 0.2. Given the susceptibility to contrast agent leakage in HGG patients, Weisskoff correction was applied to account for T1- and T2-shortening effects [16].

Finally, normalization was performed to minimize inter-subject variability by utilizing the mean perfusion values from an automatically generated normal brain tissue mask. Leakage-corrected perfusion maps, including nCBV, nCBF, and nMTT, were then calculated for each patient.

IVIM Parametric Map Generation

IVIM parametric maps were generated using the MITK diffusion (2.0.1) by fitting the IVIM data to equation 1 [17]:

$$\frac{S_b}{S_0} = fe^{-(b\times D^*)} + (1-f)e^{-(b\times D)} \quad (1)$$

where S_b is MRI signal intensity at a given b-value, S_0 is a signal intensity at a b-value equal to 0, f is the perfusion fraction, representing the fraction of the signal attributed to microcirculation, D* is pseudo-diffusion coefficient, representing the perfusion-related incoherent microcirculation, and D is true diffusion coefficient, representing the tissue's water molecule diffusion.

This model employs a two-step fitting process to produce IVIM parametric maps. In the first step, data points at higher b-values (greater than approximately 200 s/mm²) are used to estimate the D and the f. These estimated values are then held constant while the model calculates the D*.

The mono-exponential model was used to generate the Apparent Diffusion Coefficient (ADC) map. Based on an exponential relationship between signal intensity and diffusion weighting (b-value), this model estimates the ADC of water molecules within tissues. To accomplish this, it was fitted to IVIM data acquired at two specific b-values: 0 s/mm² and 1000 s/mm².

To minimize inter-subject variability in IVIM parameters, parametric map values were normalized using a Region of Interest (ROI) (25–30 mm²) placed in the Normal-Appearing White Matter (NAWM) contralateral to the lesion on T2-weighted images. FireVoxel software (build 456; https://FireVoxel.org) was used to automatically normalize IVIM maps by dividing all pixel values by the mean NAWM value.

Spectral Data Analysis

Functool software on a dedicated workstation was used to post-process the raw SV-MRS data. This involved baseline correction, frequency inversion, and phase shift adjustments. Peak areas for N-Acetyl Aspartate (NAA), Choline (Cho), and Creatine (Cr) metabolites were determined by fitting Gaussian curves to the corresponding peaks. Ratios of peak heights, including Cho/Cr, Cho/NAA, Cr/NAA, NAA/Cr, and NAA/Cho, were calculated. Finally, normalized metabolite ratios were derived. These ratios represent the concentration of each metabolite in the enhancing lesion relative to the contralateral healthy brain tissue.

Image registration

Anatomical images (Flair, T1-w, T1-w post contrast) and parametric maps of IVIM and

DSC images were meticulously registered to the T2-w images for each patient using the ITK-snap 4.2.0 software.

Enhanced lesion segmentation

The subtraction and ROI drawing tools in FireVoxel software were used to segment the enhanced lesion. By subtracting post-contrast and pre-contrast T1-weighted images, subtracted T1 images were generated that more clearly visualized the enhanced lesion. Then a Volume of Interest (VOI) was drawn on the enhanced region of the lesion in subtracted images using the ROI drawing tool in FireVoxel. Areas with necrosis, hemorrhage, or large blood vessels (visible on post-contrast T1-weighted or T2-weighted FLAIR images) were excluded from the VOI. The VOI was then transferred to the registered IVIM and DSC MRI parametric maps (Figure 1).

Statistical Analysis

Statistical Analysis was performed using SPSS (IBM SPSS Statistics, version 27.0; IBM Corporation). The mean pixel value of the VOI in IVIM MRI and DSC MRI parametric maps was calculated using FireVoxel software. For MRS data, normalized metabolite ratios were computed for each patient. Data normality was assessed using the Shapiro-Wilk test. Group comparisons between PSP and TP were conducted using independent sample t-tests for normally distributed data and Mann-Whitney U-tests for non-normally distributed data. A P-value<0.05 was considered statistically significant.

Optimal cutoff values for each parameter were determined using Receiver Operating Characteristic (ROC) curve analysis, with the Youden index applied to maximize sensitivity and specificity. Statistically significant parameters distinguishing PSP from TP were integrated into the MSS method. Each parameter was assigned a binary score (1=TP, 0=PSP) based on its cutoff value. Specifically, a score

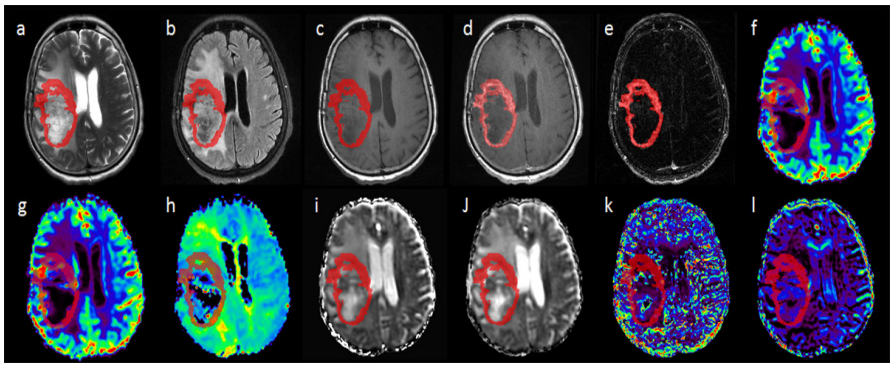

Figure 1: The multiparametric MRI protocol produced both anatomical images and parametric maps derived from DSC MRI and IVIM MRI for a representative case. The top row, arranged from left to right, displays anatomical images, including (**a**) T2-weighted, (**b**) FLAIR, (**c**) pre-contrast T1-weighted, (**d**) post-contrast T1-weighted, (**e**) subtracted T1 image, and (**f**) nCBV map. The bottom row, also arranged from left to right, presents DSC MRI and IVIM MRI maps: (**g**) nCBF map, (**h**) nMTT map, (**i**) nD map, (**j**) nADC map, (**k**) nD* map, and (**l**) nf map. The red overlay highlights the ROI within the enhancing lesion, which was used for quantitative analysis of parametric maps. (MRI: Magnetic Resonance Imaging, DSC: Dynamic Susceptibility Contrast, IVIM: Intravoxel Incoherent Motion, FLAIR: Fluid-Attenuated Inversion Recovery, nCBV: normalized Cerebral Blood Volume, nCBF: normalized Cerebral Blood Flow, nMTT: normalized Mean Transit Time, nD: normalized True Diffusion Coefficient, nADC: normalized Apparent Diffusion Coefficient, nD*: normalized Pseudo-Diffusion Coefficient, nf: normalized Perfusion Fraction, and ROI: Region of Interest.)

of 1 was assigned when a parameter exceeded its cutoff, and 0 otherwise. For parameters like nADC and nD, which have an inverse relationship with classification, the scoring was reversed: 1 was assigned if the value was below the cutoff, and 0 otherwise. Individual scores were summed to generate a sum score for each patient.

The normality of the sum score distribution was evaluated, followed by an independent sample t-test or Mann-Whitney U-test, as appropriate. Finally, the diagnostic performance of the MSS method, as well as individual MRI parameters, was assessed using ROC curve analysis. Evaluation metrics, including AUC, sensitivity, specificity, accuracy, Positive Predictive Value (PPV), and Negative Predictive Value (NPV), were calculated..

Results

Comparison of MRI parameters between PSP and TP groups

The quantitative analysis identified significant differences in multiple perfusions, diffusions, and MRS parameters between the PSP and TP groups. In DSC MRI, the TP group exhibited significantly higher mean nCBV and nCBF (*P*-value=0.001 for both), along with a significantly increased mean nMTT (*P*-value=0.029) compared to the PSP group.

In IVIM MRI, the mean normalized true diffusion coefficient (nD), and normalized Apparent Diffusion Coefficient (nADC) were significantly lower in TP (*P*=0.009 and *P*-value=0.026, respectively), while the mean normalized pseudo-diffusion coefficient (nD*) was significantly higher in TP (*P*-value=0.028). The median normalized perfusion fraction (nf) was also higher in TP; however, this difference did not reach statistical significance (*P*-value=0.64).

For MRS metabolite ratios, five normalized ratios, including Cho/Cr, Cho/NAA, Cr/NAA, NAA/Cho, and NAA/Cr were calculated for all patients. While Cho/NAA and NAA/Cho showed trends toward significance (*P*-value=0.074 and *P*-value=0.067, respectively), only normalized Cho/Cr exhibited a statistically significant difference between PSP and TP (*P*-value=0.003). Normalized Cr/NAA and NAA/Cr did not show a significant difference between PSP and TP groups (*P*-value=0.9 and *P*-value=0.6, respectively).

Box plots comparing the significantly different MRI parameters and the metabolite ratio between the two patient groups are presented in Figure 2.

Diagnostic Performance of Individual Parameters

ROC curve analysis was performed to assess the diagnostic performance of each MRI parameter, and a significant difference was observed between PSP and TP. The sensitivity, specificity, accuracy, PPV, NPV, and AUC values for these parameters are summarized in Table 2. ROC curves for these MRI parameters and the sum score from MSS are depicted in Figure 3. Among the significant MRI parameters, the highest AUC values were observed for mean nCBF and nCBV, followed by nCho/Cr and mean nD.

MSS Performance

Statistical analysis revealed that the median sum score was significantly higher in the TP group (*P*-value<0.001). ROC analysis of the sum score yielded an AUC of 0.958, with a sensitivity of 87.5% and specificity of 92.9% in identifying TP patients at a cutoff value of 4. The MSS approach demonstrated superior diagnostic performance compared to individual parameters (Table 2). Misclassification occurred in 3 of 30 patients, with one PSP case misclassified as TP and two TP cases misclassified as PSP. Table 3 provides the values of MRI parameters that significantly differed between PSP and TP groups, along with their corresponding scores for all patients. Additionally, comparisons between the AUC of MSS and individual MRI parameters

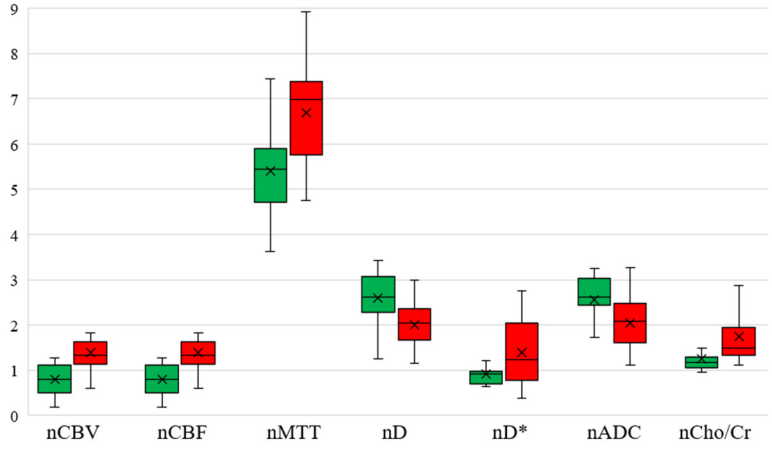

Figure 2: Boxplots illustrating the distribution of MRI parameters that showed significant differences between PSP and TP groups. The parameters include nCBV [mL/100g], nCBF [mL/100g/min], nMTT [1/sec] from DSC MRI, nD [10−3 mm^2/s], nD* [10−3 mm^2/s], nADC [10−3 mm^2/s] from IVIM MRI, and the normalized nCho/Cr from SV-MRS. Green and red boxes represent the PSP and TP groups, respectively. In each boxplot, the horizontal line within the box denotes the median, while the cross symbol represents the mean. The whiskers indicate the range of the data, highlighting the variation in each parameter between the two groups. (MRI: Magnetic Resonance Imaging, PSP: Pseudoprogression, TP: True Progression, nCBV: normalized Cerebral Blood Volume, nCBF: normalized Cerebral Blood Flow, nMTT: normalized Mean Transit Time, DSC: Dynamic Susceptibility Contrast, nD: normalized True Diffusion Coefficient, nADC: normalized Apparent Diffusion Coefficient, nD*: normalized Pseudo-Diffusion Coefficient, IVIM: Intravoxel Incoherent Motion, nCho/Cr: normalized Choline to Creatine ratio, SV-MRS: Single Voxel Magnetic Resonance Spectroscopy.)

revealed that MSS significantly outperformed nMTT (*P*-value=0.015), nD (*P*-value=0.007), nD* (*P*=0.014), and nADC (*P*=0.006). However, its AUC did not differ significantly from nCBV (*P*=0.074), nCBF (*P*=0.09), or nCho/Cr (*P*=0.074).

Discussion

Although pathological sampling remains the gold standard for differentiating PSP from true progression TP in high-grade glioma, its invasiveness and potential for sampling error limit its widespread applicability [18]. As a result, follow-up conventional MRI is more commonly employed. However, conventional MRI lacks sufficient specificity to reliably distinguish between PSP and TP, as both conditions can exhibit overlapping imaging features, including mass effect, perilesional edema, and contrast enhancement, due to blood-brain barrier disruption [5]. To overcome these limitations, many studies have proposed that integrating multiple advanced MRI techniques within a multiparametric imaging protocol could help by providing complementary information for lesion characterization [9].

In this study, we employed a multiparametric MRI approach incorporating DSC MRI, IVIM MRI, and MRS. Following image acquisition, MRI parameters were extracted for each technique, and their mean values within a VOI delineated on the enhancing region of contrast-enhanced T1-weighted images were compared between the PSP and TP groups. Statistically significant parameters were identified and subsequently integrated using the

Table 2: Diagnostic performance of individual MRI parameters and the MSS for distinguishing PSP from TP. The table presents Sensitivity, Specificity, Accuracy, PPV, NPV, and the AUC for each parameter, including mean nCBV, nCBF, nMTT, nD, nD*, nADC, and median nCho/Cr. MSS, which integrates multiple parameters, demonstrates the highest overall diagnostic performance.

	nCBV	nCBF	nMTT	nD	nD*	nADC	nCho/Cr	MSS
Sensitivity	81.3%	62.5%	87.5%	87.5%	56.3%	68.8%	81.3%	87.5%
Specificity	78.6%	100%	71.4%	64.3%	92.9%	78.6%	78.6%	92.9%
Accuracy	80%	80%	80%	76.7%	73.3%	73.3%	80%	90.0%
PPV	81.3%	100%	77.8%	73.7%	90%	78.6%	81.3%	93.3%
NPV	78.6%	70%	83.3%	81.8%	65%	68.8%	78.6%	86.7%
AUC (95% CI)	0.853 (0.72-0.99)	0.857 (0.73-0.99)	0.746 (0.56-0.93)	0.781 (0.61-0.95)	0.692 (0.49-0.89)	0.741 (0.55-0.93)	0.817 (0.66-0.97)	0.958 (0.89-1.00)

MRI: Magnetic Resonance Imaging, MSS: Multiparametric Scoring System, PSP: Pseudoprogression, TP: True Progression, PPV: Positive Predictive Value, NPV: Negative Predictive Value, AUC: Area Under the Curve, nCBV: normalized Cerebral Blood Volume, nCBF: normalized Cerebral Blood Flow, nMTT: normalized Mean Transit Time, nD: normalized True Diffusion Coefficient, nD*: normalized Pseudo-Diffusion Coefficient, nADC: normalized Apparent Diffusion Coefficient, nCho/Cr: normalized Choline to Creatine ratio, CI: Confidence Intervals

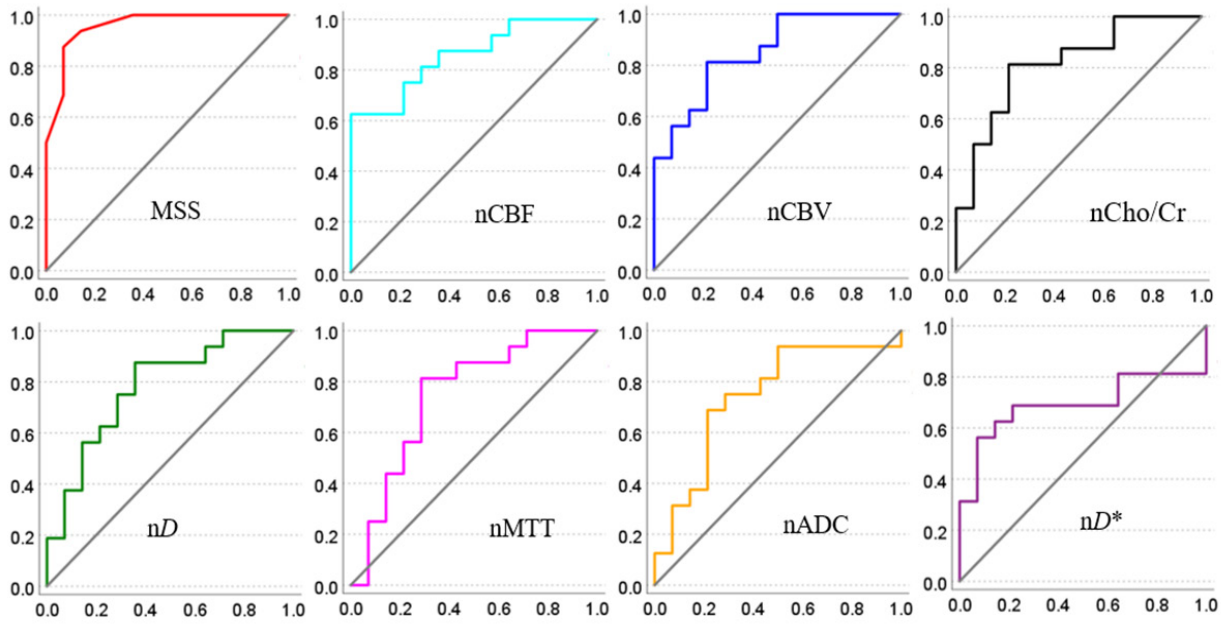

Figure 3: ROC curves for PSP from TP using different MRI parameters and the MSS. The ROC curves are shown for MSS, nCBV, nCBF, nMTT, nD, nD*, nADC, and the nCho/Cr. The Y-axis represents Sensitivity, while the X-axis represents 1-Specificity. The diagonal gray line represents reference line for the ROC curve (AUC=0.5). (ROC: Receiver operating characteristic, AUC: Area Under the Curve, PSP: Pseudoprogression, TP: True Progression, MSS: Multiparametric Scoring System, nCBF: normalized Cerebral Blood Flow, nCBV: normalized Cerebral Blood Volume, nCho/Cr: normalized Choline to Creatine ratio, nD: normalized True Diffusion Coefficient, nMTT: normalized Mean Transit Time, nADC: normalized Apparent Diffusion Coefficient, nD*: normalized Pseudo-Diffusion Coefficient.)

Table 3: MRI parameters involved in MSS approach including nCBV [mL/100g], nCBF [mL/100g/min], nMTT [1/sec], nD [10−3 mm^2/s], nD* [10−3 mm^2/s], nADC [10−3 mm^2/s], and the nCho/Cr. Each parameter's score was determined based on whether it met the cutoff value. The sum score for each patient is calculated by adding the MRI parameters score in each row. Labels in the first column served as the reference method for patient categorization. The last column presents patient categorization based on the sum score obtained from the MSS. Patient categorization was determined using a sum score cutoff value of 4, as established by ROC analysis of the MSS approach.

ID	Label	nCBV-(score), cutoff =1.21	nCBF-(score), cutoff =1.28	nMTT-(score), cutoff =5.71	nD-(score), cutoff =2.52	nD*-(score), cutoff =1.21	nADC-(score), cutoff =2.38	nCho/Cr-(score), cutoff =1.32	Sum Score, cutoff =4	Categorized based on the Sum Score from the MSS
1	PSP	0.55-(0)	0.51-(0)	4.65-(0)	2.37-(1)	0.67-(0)	2.45-(0)	1.24-(0)	1	PSP
2	PSP	0.80-(0)	0.69-(0)	7.09-(1)	2.64-(0)	0.89-(0)	2.45-(0)	1.35-(1)	2	PSP
3	PSP	0.80-(0)	0.82-(0)	4.89-(0)	3.37-(0)	0.70-(0)	3.24-(0)	1.04-(0)	0	PSP
4	PSP	1.21-(0)	1.13-(0)	5.96-(1)	1.73-(1)	0.98-(0)	1.72-(1)	1.32-(0)	3	PSP
5	PSP	1.33-(1)	1.26-(0)	5.48-(0)	2.60-(0)	0.95-(0)	2.82-(0)	0.98-(0)	1	PSP
6	PSP	0.57-(0)	0.49-(0)	5.13-(0)	2.12-(1)	1.21-(0)	1.95-(1)	0.95-(0)	2	PSP
7	PSP	0.44-(0)	0.41-(0)	4.27-(0)	3.42-(0)	0.91-(0)	3.22-(0)	2.18-(1)	1	PSP
8	PSP	0.60-(0)	0.45-(0)	3.63-(0)	3.28-(0)	1.71-(1)	3.09-(0)	1.18-(0)	1	PSP
9	PSP	0.88-(0)	0.78-(0)	5.52-(0)	2.25-(1)	0.96-(0)	2.43-(0)	1.22-(0)	1	PSP
10	PSP	1.20-(0)	1.08-(0)	5.68-(0)	2.70-(0)	0.63-(0)	2.74-(0)	1.04-(0)	0	PSP
11	PSP	1.48-(1)	1.22-(0)	9.10-(1)	2.59-(0)	0.63-(0)	2.59-(0)	1.10-(0)	2	PSP
12	PSP	1.21-(0)	0.79-(0)	5.41-(0)	2.79-(0)	0.90-(0)	2.65-(0)	1.16-(0)	0	PSP
13	PSP	1.36-(1)	1.21-(0)	7.45-(1)	1.24-(1)	1.02-(0)	1.27-(1)	1.49-(1)	5	TP
14	PSP	0.21-(0)	0.19-(0)	1.41-(0)	3.15-(0)	0.70-(0)	3.20-(0)	1.18-(0)	0	PSP
15	TP	1.70-(1)	1.68-(1)	4.75-(0)	1.23-(1)	0.37-(0)	1.24-(1)	1.87-(1)	5	TP
16	TP	1.43-(1)	1.34-(1)	7.33-(1)	1.49-(1)	1.23-(1)	1.42-(1)	1.20-(0)	6	TP
17	TP	1.45-(1)	1.36-(1)	7.14-(1)	2.04-(1)	1.17-(0)	2.13-(1)	1.11-(0)	5	TP
18	TP	1.35-(1)	1.30-(1)	5.76-(1)	2.33-(1)	0.59-(0)	2.33-(1)	2.18-(1)	6	TP
19	TP	2.23-(1)	1.83-(1)	8.93-(1)	1.73-(1)	2.75-(1)	1.66-(1)	2.87-(1)	7	TP
20	TP	0.91-(0)	0.83-(0)	5.74-(1)	2.76-(0)	1.00-(0)	2.59-(0)	2.95-(1)	2	PSP
21	TP	2.88-(1)	2.81-(1)	5.48-(0)	1.71-(1)	2.03-(1)	1.80-(1)	2.66-(1)	6	TP
22	TP	1.50-(1)	1.34-(1)	7.23-(1)	1.19-(1)	0.79-(0)	1.34-(1)	1.33-(1)	6	TP
23	TP	1.81-(1)	1.60-(1)	7.08-(1)	2.99-(0)	2.10-(1)	3.27-(0)	1.15-(0)	4	TP
24	TP	0.85-(0)	0.71-(0)	5.94-(1)	2.03-(1)	2.44-(1)	1.97-(1)	1.81-(1)	5	TP
25	TP	1.87-(1)	1.52-(1)	8.36-(1)	1.95-(1)	2.25-(1)	2.04-(1)	1.34-(1)	7	TP
26	TP	1.26-(1)	1.16-(0)	5.86-(1)	2.16-(1)	1.37-(1)	2.23-(1)	1.43-(1)	6	TP
27	TP	0.83-(0)	0.59-(0)	8.04-(1)	2.45-(1)	0.56-(0)	2.61-(0)	1.59-(1)	3	PSP
28	TP	1.27-(1)	1.16-(0)	4.98-(0)	2.29-(1)	1.55-(1)	2.62-(0)	1.32-(1)	4	TP
29	TP	1.78-(1)	1.81-(1)	7.50-(1)	1.16-(1)	1.21-(1)	1.12-(1)	1.49-(1)	7	TP
30	TP	1.22-(1)	1.08-(0)	6.89-(1)	2.41-(1)	0.76-(0)	2.45-(0)	1.48-(1)	4	TP

MRI: Magnetic Resonance Imaging, MSS: Multiparametric Scoring System, nCBV: normalized Cerebral Blood Volume, nCBF: normalized Cerebral Blood Flow, nMTT: normalized Mean Transit Time, nD: normalized True Diffusion Coefficient, nD*: normalized Pseudo-Diffusion Coefficient, nADC: normalized Apparent Diffusion Coefficient, nCho/Cr: normalized Choline to Creatine ratio, ROC: Receiver Operating Characteristic, ID: Identification Number, PSP: Pseudoprogression, TP: True Progression

MSS method.

The main findings of this study indicate that the MSS approach effectively integrates multiple MRI parameters by assigning them an appropriate score of 0 or 1, leveraging their complementary diagnostic value to improve the differentiation between PSP and TP in high-grade glioma patients. As presented in Table 2, the MSS achieved a high AUC of 0.958, with a sensitivity of 87.5% and specificity of 92.9%, resulting in an overall classification accuracy of 90%, showing MSS accurately identified 87.5% of TP cases and 92.9% of PSP cases in this study. Overall, MSS correctly classified 27 out of 30 patients based on the reference standard used. This accuracy surpasses that of any individual MRI parameter included in the analysis.

The MSS has the potential to provide a more comprehensive view of the underlying disease process. Individual MRI parameters, such as nCBV or ADC, capture specific physiological or structural features, such as vascularity or cellular density. However, these single metrics may not fully reflect the multifaceted nature of PSP and TP, where overlapping or complementary changes in perfusion, microstructure, and metabolism often coexist. MSS could overcome this limitation by aggregating scores across multiple parameters. In addition to a comprehensive assessment, MSS enhances diagnostic reliability by addressing the inherent variability of individual MRI parameters. Each parameter is susceptible to technical or biological fluctuations, which can lead to inconsistent or unreliable classifications when used alone. By summing scores across multiple parameters, MSS effectively averages out these inconsistencies, resulting in a reliable diagnostic framework. Therefore, in cases where individual parameters yield ambiguous or conflicting results, the composite nature of MSS allows it to refine classifications by leveraging the collective strength of multiple signals.

Our results align with previous studies that have shown multiparametric MRI improves differentiation between treatment-related effects and true progression. A study by Shan et al. utilized logistic regression to combine parameters from IVIM and DSC MRI to differentiate tumor recurrence from radiation brain injury [19]. The combination of MRI parameters resulted in an increased AUC (0.891) compared to individual parameters from DSC and IVIM MRI. Jajodia et al. explored the use of perfusion and diffusion MRI parameters to distinguish radiation-induced necrosis from tumor recurrence in GBM patients. Their logistic regression analysis revealed that a combination of rCBV and ADC provided superior diagnostic accuracy (AUC=0.93) compared to using either parameter alone [20]. Di Costanzo et al. explored the effectiveness of a multiparametric 3T MRI approach to differentiate between recurrent glioblastoma multiforme and radiation injury, incorporating MRS, diffusion weighted MRI (DWI), and DSC MRI. Their study demonstrated that combining metabolite ratios from MRS, ADC from DWI, and rCBV from DSC MRI through discriminant analysis significantly enhanced diagnostic accuracy, achieving a classification accuracy of 96.6% [21].

While many studies in this field have utilized logistic regression to combine multiple MRI parameters [19, 22, 23], the MSS achieved a level of diagnostic accuracy comparable to these more complex approaches, albeit with a simpler and more direct method. An additional advantage of the MSS approach lies in its ability to generate a final cutoff value that considers all significant MRI parameters simultaneously, providing a tangible and easily interpretable threshold for clinical decision-making. This feature enhances the method's utility in clinical practice, as it provides a clear threshold for distinguishing between conditions, a feature not inherently available when employing methods like logistic regression.

The integration of MRI parameters into a

scoring system has garnered attention in recent studies [24, 25]. Accordingly, several studies have developed specific scoring systems to address various challenges [26-28]. For instance, Hosur et al. proposed a multiparametric MRI-based scoring system to predict Isocitrate Dehydrogenase (IDH) mutation status [26], while Kang et al. introduced a streamlined MRI-based scoring system for predicting both IDH mutation and 1p/19q codeletion in contrast-enhancing gliomas [27]. Additionally, Kanazawa et al. established an imaging scoring system for the preoperative diagnosis of essential molecular markers in lower-grade gliomas [28]. Collectively, these studies highlighted the growing versatility and potential of imaging-based scoring systems in enhancing clinical decision-making across diverse scenarios. In line with these findings, MSS has been successfully applied to evaluate Parkinson's disease [29, 30], assess peritumoral brain swelling in meningiomas [31], and distinguish dementia with Lewy bodies from Alzheimer's disease [32], further showcasing its versatility.

The evaluation of individual MRI parameters revealed significantly elevated nCBV, nCBF, nMTT, nD*, and normalized Cho/Cr, as well as decreased nD and nADC in the TP group compared to the PSP group, which is in line with previous studies [19-21]. Moreover, DSC MRI showed the highest diagnostic performance, followed by MRS and IVIM MRI (Table 2). This result is consistent with previous studies that have demonstrated the superiority of DSC MRI over MRS and DWI techniques in distinguishing PSP from TP [21, 23]. However, other studies have reported conflicting findings, suggesting that MRS outperforms both DSC and diffusion MRI in differentiating PSP from TP [33, 34]. The observed differences may be attributed to using single-voxel MRS. A key factor influencing this choice was the frequent presence of altered brain morphology in our patient cohort due to prior surgery and radiotherapy. This structural distortion, particularly around the enhanced region, often led to significant magnetic field inhomogeneities and susceptibility artifacts, which can degrade the spectrum quality in MRS. To address this challenge, SV-MRS was selected for its flexibility in voxel placement, enabling more precise positioning in areas with better field homogeneity. However, using SV-MRS may have reduced sensitivity to metabolic heterogeneity compared to multi-voxel approaches used in other studies. Accordingly, the superior diagnostic performance reported by El-Abtah et al. [33] and Jena et al. [34] may be attributed to their use of multi-voxel MRS, which provides spatially resolved metabolic data and better captures metabolic heterogeneity.

Although consistent with previous studies, where the perfusion fraction (f) parameter was higher in the TP group than in the PSP group, it did not show a significant difference between the two groups in our study. This discrepancy may be attributed to several factors, influencing IVIM parameter estimation, including the choice of b-values, signal-to-noise ratio, and fitting methods. Additionally, f represents a relatively small component of the IVIM signal, typically less than 5% in brain tissue [17], making it more susceptible to noise and measurement variability compared to D or D* [35]. Another important distinction is that we computed the normalized f value, while previous studies reported its absolute value. Normalization may have altered the parameter's sensitivity to perfusion-related differences between PSP and TP, which could explain the observed findings.

The present study has several limitations, as follows: 1) the relatively small sample size may limit the generalizability of our findings, as a larger cohort could improve the reliability and statistical power of the results and 2) the absence of histological confirmation for all cases represents a limitation. While pathological sampling remains the gold standard for diagnosis, follow-up MRI is widely utilized in clinical practice to monitor treatment response

due to the invasive nature of repeat biopsies and their associated risks. Additionally, even when biopsies are performed, they may fail to fully capture the spatial heterogeneity of HGG, potentially leading to sampling error [36]. Notably, in our cohort, the five cases with histopathological confirmation were consistent with the MRI-based classification, supporting the reliability of our approach. Nonetheless, future studies involving larger cohorts with histopathological confirmation would further enhance the robustness of these findings.

A third limitation stems from the Echo-Planar Imaging (EPI)-based nature of DSC MRI and IVIM MRI sequences, which are particularly vulnerable to susceptibility artifacts caused by magnetic field inhomogeneities. This effect is more pronounced in patients with enhanced lesions near the skull base or paranasal sinuses, potentially leading to image distortions [37]. Such distortions may result in spatial misalignment between the enhanced lesion and the 3D ROI drawn on anatomical MRI images, thereby affecting parameter quantification in IVIM and DSC MRI. To mitigate these challenges, selecting hotspot ROIs, focusing on the most enhanced regions in post-contrast T1-weighted images, may offer advantages over 3D ROIs that encompass the entire enhanced lesion, as it reduces the impact of susceptibility-induced artifacts on the extracted imaging parameters.

Another limitation of our study is that the MSS approach assigns equal weights to each MRI parameter in the sum score calculation. However, prior reviews of multiparametric MRI studies and the findings of this study indicate that different MRI parameters contribute variably to diagnostic performance. Therefore, assigning optimized weights to parameters derived from different advanced MRI techniques could potentially enhance classification accuracy. Future studies should explore weighted scoring systems to refine the MSS approach further and improve its clinical applicability.

Conclusion

The findings of this study underscore the effectiveness of integrating multiparametric MRI with the MSS approach in differentiating between pseudoprogression and true progression in high-grade glioma patients. By summing scores across multiple parameters, MSS effectively averages out inconsistencies among different MRI metrics, ultimately improving patient classification performance. While promising, the MSS approach relies on binary cutoff values, which may oversimplify borderline cases. A weighted scoring system could enhance differentiation and classification accuracy. Future studies should explore optimized parameter weighting to improve the MSS approach's clinical applicability.

Authors' Contribution

The study was conceptualized and designed by M. Ghorbani and MA. Oghabian. Imaging data acquisition was carried out by S. Raminfard and M. Farsi. Clinical evaluation, determination of patient status, and contributions to data analysis were conducted by N. Sadighi and M. Farzin. Data analysis and interpretation were primarily performed by M. Ghorbani, with guidance and supervision from MA. Oghabian. All authors participated in interpreting the findings, critically reviewed the manuscript, and contributed to its final version.

Ethical Approval

The Ethics Committee of Tehran University of Medical Sciences approved the protocol of the study (Ethic cod: IR.TUMS.MEDICINE.REC.1400.621).

Informed Consent

All patients were duly informed, and consent forms were obtained for the utilization of their data in the context of our research.

Funding

This work is supported by the Tehran

University of Medical Science (grant number: 1400-3-373-54834).

Conflict of Interest

None

Data Availability Statement

The training sets (TS1, TS2, and TS3) described in this study and the code generating the results are publicly available at https://github.com/labCOI/microscopy_illumination_correction.

References

1. Manning P, Daghighi S, Rajaratnam MK, Parthiban S, Bahrami N, Dale AM, et al. Differentiation of progressive disease from pseudoprogression using 3D PCASL and DSC perfusion MRI in patients with glioblastoma. *J Neurooncol.* 2020;**147**(3):681-90. doi: 10.1007/s11060-020-03475-y. PubMed PMID: 32239431.
2. Le Fèvre C, Constans JM, Chambrelant I, Antoni D, Bund C, Leroy-Freschini B, et al. Pseudoprogression versus true progression in glioblastoma patients: A multiapproach literature review. Part 2 - Radiological features and metric markers. *Crit Rev Oncol Hematol.* 2021;**159**:103230. doi: 10.1016/j.critrevonc.2021.103230. PubMed PMID: 33515701.
3. Thust SC, Van Den Bent MJ, Smits M. Pseudoprogression of brain tumors. *J Magn Reson Imaging.* 2018;**48**(3):571-89. doi: 10.1002/jmri.26171. PubMed PMID: 29734497. PubMed PMCID: PMC6175399.
4. Kruser TJ, Mehta MP, Robins HI. Pseudoprogression after glioma therapy: a comprehensive review. *Expert Rev Neurother.* 2013;**13**(4):389-403. doi: 10.1586/ern.13.7. PubMed PMID: 23545054.
5. Ryken TC, Aygun N, Morris J, Schweizer M, Nair R, Spracklen C, et al. The role of imaging in the management of progressive glioblastoma : a systematic review and evidence-based clinical practice guideline. *J Neurooncol.* 2014;**118**(3):435-60. doi: 10.1007/s11060-013-1330-0. PubMed PMID: 24715656.
6. Liu ZC, Yan LF, Hu YC, Sun YZ, Tian Q, Nan HY, et al. Combination of IVIM-DWI and 3D-ASL for differentiating true progression from pseudoprogression of Glioblastoma multiforme after concurrent chemoradiotherapy: study protocol of a prospective diagnostic trial. *BMC Med Imaging.* 2017;**17**(1):10. doi: 10.1186/s12880-017-0183-y. PubMed PMID: 28143434. PubMed PMCID: PMC5286785.
7. Liao D, Liu YC, Liu JY, Wang D, Liu XF. Differentiating tumour progression from pseudoprogression in glioblastoma patients: a monoexponential, biexponential, and stretched-exponential model-based DWI study. *BMC Med Imaging.* 2023;**23**(1):119. doi: 10.1186/s12880-023-01082-7. PubMed PMID: 37697237. PubMed PMCID: PMC10494379.
8. Rabinov JD, Lee PL, Barker FG, Louis DN, Harsh GR, Cosgrove GR, et al. In vivo 3-T MR spectroscopy in the distinction of recurrent glioma versus radiation effects: initial experience. *Radiology.* 2002;**225**(3):871-9. doi: 10.1148/radiol.2253010997. PubMed PMID: 12461273.
9. Gonçalves FG, Chawla S, Mohan S. Emerging MRI Techniques to Redefine Treatment Response in Patients With Glioblastoma. *J Magn Reson Imaging.* 2020;**52**(4):978-97. doi: 10.1002/jmri.27105. PubMed PMID: 32190946. PubMed PMCID: PMC7492394.
10. Suh CH, Kim HS, Jung SC, Choi CG, Kim SJ. Multiparametric MRI as a potential surrogate endpoint for decision-making in early treatment response following concurrent chemoradiotherapy in patients with newly diagnosed glioblastoma: a systematic review and meta-analysis. *Eur Radiol.* 2018;**28**(6):2628-38. doi: 10.1007/s00330-017-5262-5. PubMed PMID: 29374321.
11. Winfield JM, Payne GS, Weller A, DeSouza NM. DCE-MRI, DW-MRI, and MRS in Cancer: Challenges and Advantages of Implementing Qualitative and Quantitative Multi-parametric Imaging in the Clinic. *Top Magn Reson Imaging.* 2016;**25**(5):245-54. doi: 10.1097/RMR.0000000000000103. PubMed PMID: 27748710. PubMed PMCID: PMC5081190.
12. Matsusue E, Fink JR, Rockhill JK, Ogawa T, Maravilla KR. Distinction between glioma progression and post-radiation change by combined physiologic MR imaging. *Neuroradiology.* 2010;**52**(4):297-306. doi: 10.1007/s00234-009-0613-9. PubMed PMID: 19834699.
13. Hu YC, Yan LF, Han Y, Duan SJ, Sun Q, Li GF, et al. Can the low and high b-value distribution influence the pseudodiffusion parameter derived from IVIM DWI in normal brain? *BMC Med Imaging.* 2020;**20**(1):14. doi: 10.1186/s12880-020-0419-0. PubMed PMID: 32041549. PubMed PMCID: PMC7011602.
14. Cecil KM. Proton magnetic resonance spectroscopy: technique for the neuroradiologist. *Neuroimag-*

ing Clin N Am. 2013;**23**(3):381-92. doi: 10.1016/j.nic.2012.10.003. PubMed PMID: 23928195. PubMed PMCID: PMC3748933.

15. Boer VO, Klomp DW. Technical Considerations for Multivoxel Approaches and Magnetic Resonance Spectroscopic Imaging. In: Stagg C, Rothman D, editors. Magnetic Resonance Spectroscopy. San Diego: Academic Press; 2014. p. 31-9.
16. Shiroishi MS, Castellazzi G, Boxerman JL, D'Amore F, Essig M, Nguyen TB, et al. Principles of T2 *-weighted dynamic susceptibility contrast MRI technique in brain tumor imaging. *J Magn Reson Imaging.* 2015;**41**(2):296-313. doi: 10.1002/jmri.24648. PubMed PMID: 24817252.
17. Le Bihan D. What can we see with IVIM MRI? *Neuroimage*. 2019;**187**:56-67. doi: 10.1016/j.neuroimage.2017.12.062. PubMed PMID: 29277647.
18. Melguizo-Gavilanes I, Bruner JM, Guha-Thakurta N, Hess KR, Puduvalli VK. Characterization of pseudoprogression in patients with glioblastoma: is histology the gold standard? *J Neurooncol.* 2015;**123**(1):141-50. doi: 10.1007/s11060-015-1774-5. PubMed PMID: 25894594. PubMed PMCID: PMC4780341.
19. Shan MY, Yang GQ, Qin JB. Preliminary study of DSC-MRI and IVIM in differentiating postoperative recurrence and radiation brain injury of high-grade glioma. Chin J Magn Reson Imaging. 2020;11(5):326-31.
20. Jajodia A, Goel V, Goyal J, Patnaik N, Khoda J, Pasricha S, Gairola M. Combined Diagnostic Accuracy of Diffusion and Perfusion MR Imaging to Differentiate Radiation-Induced Necrosis from Recurrence in Glioblastoma. *Diagnostics (Basel)*. 2022;**12**(3):718. doi: 10.3390/diagnostics12030718. PubMed PMID: 35328270. PubMed PMCID: PMC8947286.
21. Di Costanzo A, Scarabino T, Trojsi F, Popolizio T, Bonavita S, de Cristofaro M, et al. Recurrent glioblastoma multiforme versus radiation injury: a multiparametric 3-T MR approach. *Radiol Med.* 2014;**119**(8):616-24. doi: 10.1007/s11547-013-0371-y. PubMed PMID: 24408041.
22. Nael K, Bauer AH, Hormigo A, Lemole M, Germano IM, Puig J, Stea B. Multiparametric MRI for Differentiation of Radiation Necrosis From Recurrent Tumor in Patients With Treated Glioblastoma. *AJR Am J Roentgenol*. 2018;**210**(1):18-23. doi: 10.2214/AJR.17.18003. PubMed PMID: 28952810.
23. Quan G, Zhang K, Liu Y, Ren JL, Huang D, Wang W, Yuan T. Role of Dynamic Susceptibility Contrast Perfusion MRI in Glioma Progression Evaluation. *J Oncol.* 2021;**2021**:1696387. doi: 10.1155/2021/1696387. PubMed PMID: 33628239. PubMed PMCID: PMC7886570.
24. Booth TC, Wiegers EC, Warnert EAH, Schmainda KM, Riemer F, Nechifor RE, et al. High-Grade Glioma Treatment Response Monitoring Biomarkers: A Position Statement on the Evidence Supporting the Use of Advanced MRI Techniques in the Clinic, and the Latest Bench-to-Bedside Developments. Part 2: Spectroscopy, Chemical Exchange Saturation, Multiparametric Imaging, and Radiomics. *Front Oncol.* 2022;**11**:811425. doi: 10.3389/fonc.2021.811425. PubMed PMID: 35340697. PubMed PMCID: PMC8948428.
25. Chuang MT, Liu YS, Tsai YS, Chen YC, Wang CK. Differentiating Radiation-Induced Necrosis from Recurrent Brain Tumor Using MR Perfusion and Spectroscopy: A Meta-Analysis. *PLoS One*. 2016;**11**(1):e0141438. doi: 10.1371/journal.pone.0141438. PubMed PMID: 26741961. PubMed PMCID: PMC4712150.
26. Hosur B, Ahuja CK, Singla N, Gupta K, Singh P. Advanced multiparametric MRI-based scoring for isocitrate dehydrogenase mutation prediction of gliomas. *Pol J Radiol.* 2022;**87**:e626-34. doi: 10.5114/pjr.2022.121549. PubMed PMID: 36532252. PubMed PMCID: PMC9749783.
27. Kang KM, Song J, Choi Y, Park C, Park JE, Kim HS, et al. MRI Scoring Systems for Predicting Isocitrate Dehydrogenase Mutation and Chromosome 1p/19q Codeletion in Adult-type Diffuse Glioma Lacking Contrast Enhancement. *Radiology.* 2024;**311**(2):e233120. doi: 10.1148/radiol.233120. PubMed PMID: 38713025.
28. Kanazawa T, Fujiwara H, Takahashi H, Nishiyama Y, Hirose Y, Tanaka S, et al. Imaging scoring systems for preoperative molecular diagnoses of lower-grade gliomas. *Neurosurg Rev.* 2019;**42**(2):433-41. doi: 10.1007/s10143-018-0981-x. PubMed PMID: 29700705.
29. Matsusue E, Fujihara Y, Tanaka K, Aozasa Y, Shimoda M, Nakayasu H, et al. The Utility of the Combined Use of 123I-FP-CIT and 123I-MIBG Myocardial Scintigraphy in Differentiating Parkinson's Disease from Other Parkinsonian Syndromes. *Yonago Acta Med*. 2018;**61**(2):117-27. doi: 10.33160/yam.2018.06.004. PubMed PMID: 29946218. PubMed PMCID: PMC6015794.
30. Matsusue E, Fujihara Y, Tanaka K, Aozasa Y, Shimoda M, Nakayasu H, et al. The utility of the combined use of 123I-FP-CIT SPECT and neuromelanin MRI in differentiating Parkinson's disease from other parkinsonian syn-

dromes. *Acta Radiol.* 2019;**60**(2):230-8. doi: 10.1177/0284185118778871. PubMed PMID: 29804474.

31. Higaki F, Inoue S, Oda W, Matsusue E, Hiraki T. MRI multiparametric scoring system for pial blood supply of intracranial meningiomas. *Acta Radiol Open*. 2022;**11**(4):20584601221091208. doi: 10.1177/20584601221091208. PubMed PMID: 35425642. PubMed PMCID: PMC9003652.
32. Matsusue E, Inoue C, Shimoda M, Nakamura T, Matsumoto S, Matsumoto K, et al. Utility of combining multiple parameters of 123I-IMP SPECT and voxel-based morphometry MRI using a multiparametric scoring system for differentiating dementia with Lewy bodies from Alzheimer's disease. *Acta Radiol.* 2024;**65**(7):825-34. doi: 10.1177/02841851241253775. PubMed PMID: 38785068.
33. El-Abtah ME, Talati P, Fu M, Chun B, Clark P, Peters A, et al. Magnetic resonance spectroscopy outperforms perfusion in distinguishing between pseudoprogression and disease progression in patients with glioblastoma. *Neurooncol Adv.* 2022;**4**(1):1-10. doi: 10.1093/noajnl/vdac128. PubMed PMID: 36071927. PubMed PMCID: PMC9446677.
34. Jena A, Taneja S, Jha A, Damesha NK, Negi P, Jadhav GK, et al. Multiparametric Evaluation in Differentiating Glioma Recurrence from Treatment-Induced Necrosis Using Simultaneous 18F-FDG-PET/MRI: A Single-Institution Retrospective Study. *AJNR Am J Neuroradiol.* 2017;**38**(5):899-907. doi: 10.3174/ajnr.A5124. PubMed PMID: 28341716. PubMed PMCID: PMC7960371.
35. Merisaari H, Federau C. Signal to noise and b-value analysis for optimal intra-voxel incoherent motion imaging in the brain. *PLoS One.* 2021;**16**(9):e0257545. doi: 10.1371/journal.pone.0257545. PubMed PMID: 34555054. PubMed PMCID: PMC8459980.
36. Wang L, Wei L, Wang J, Li N, Gao Y, Ma H, et al. Evaluation of perfusion MRI value for tumor progression assessment after glioma radiotherapy: A systematic review and meta-analysis. *Medicine (Baltimore).* 2020;**99**(52):e23766. doi: 10.1097/MD.0000000000023766. PubMed PMID: 33350761. PubMed PMCID: PMC7769293.
37. Stäb D, Bollmann S, Langkammer C, Bredies K, Barth M. Accelerated mapping of magnetic susceptibility using 3D planes-on-a-paddlewheel (POP) EPI at ultra-high field strength. *NMR Biomed.* 2017;**30**(4):e3620. doi: 10.1002/nbm.3620. PubMed PMID: 27763692.